Extracellular potentials generated by axonal projections are shaped by patterns of bifurcations and terminations

Thomas McColgan, Hermann Wagner, Richard Kempter

September 15, 2015

Introduction

Extracellular field potentials (EFPs) in the brain were long thought to be primarily synaptic in origin (Buzsáki et al., 2012). The study of the fields is relevant for the interpretation of data collected with measurement methods which rely on the extracellular field potential (Brette and Destexhe, 2012). Extracellular fields are also at the base of many noninvasive measurement methods (Nunez and Srinivasan, 2006), where the underlying mechanisms of far field generation are often poorly understood (Rattay and Danner, 2014).

Many modelling studies focus on the extracellular fields induced by currents on the dendrites and soma of the postsynaptic neuron (Holt and Koch, 1999; Gold et al., 2006; Lindén et al., 2010, 2011; Einevoll et al., 2013). However, a number of recent data analysis and modeling studies have revealed that active, non-synaptic membrane currents can play a role in generating EFPs (Schomburg et al., 2012; Reimann et al., 2013; Anastassiou et al., 2015).

The aim of this study is to understand how the EFP is influenced by the anatomical structure of the axons. In particular, we explain how typical projection patterns in which an axon bundle widens and then terminates in its projection area affect the EFP. Such axon bundles, sometimes called nerves or facicles, exist throughout the peripheral and central nervous system (Nornes and Das, 1972; Goodman et al., 1984; Hentschel and Ooyen, 1999; Kandel et al., 2000). The white matter of the brain can be viewed as an agglomeration of such bundles (Schüz and Braitenberg, 2002).

It has been shown (Kuokkanen et al., 2010; Denker et al., 2011; Lindén et al., 2011) that with sufficient spatial and temporal organization extracellular fields of axonal and synaptic sources can reach strengths on the order of several mV. Here we extend this finding to include more general axon bundles, including those receiving input with less temporal precision.

We characterize three principal effects of axon bundle structure on the EFP. These effects are elaborations of the properties described in past (Plonsey, 1977; Gydikov and Trayanova, 1986; Gydikov et al., 1986) for peripheral nerves. We find that the low-frequency components of the EFP are governed by the local density of bifurcations and terminations. The high-frequency components are governed by the local fiber density. Furthermore we show that the low-frequency components exceed the high-frequency components in spatial reach.

We demonstrate these properties using two models of varying complexity, both of them based on a forward model of the extracellular field potential (Holt and Koch, 1999; Gold et al., 2006). The

first model includes a detailed multicompartment model of the axon population. The second is an analytically tractable simplification of a generic bundle of axons. Finally, we demonstrate the properties in real data using as a set of in-vivo electrophysiological recordings from the barn owl brain stem.

- Some more refs to add: Ray Maunsell 2011, Belluscio 2012, Weiss 2010, rall, Rinzel, Goldwyn, telenzuk
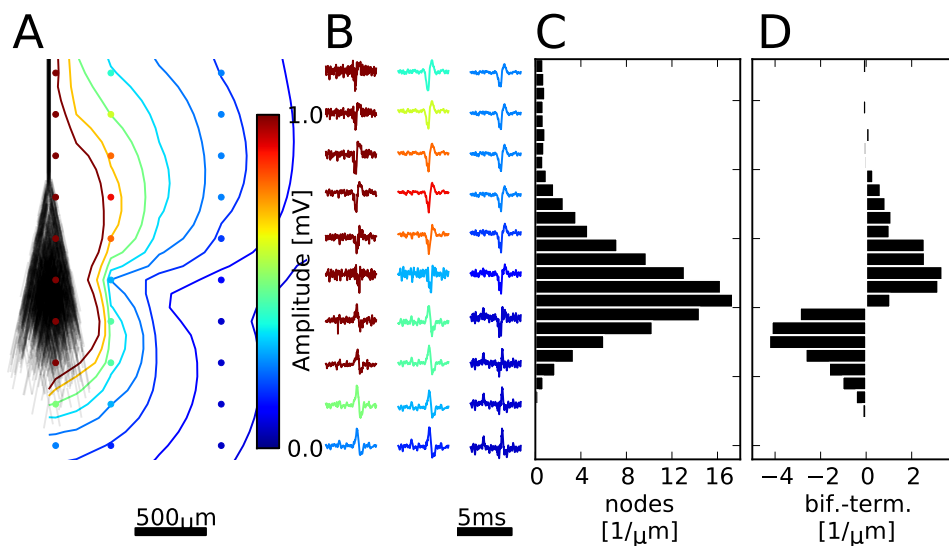
Results

Figure 1: Axonal projections generate a dipole-like extracellular field potential. Extracellular evoked potential due to a pulse of activity in a generic fiber bundle. (**A**) shows the structure of the bundle, next to (**B**) EFP responses at various locations, indicated by colored dots. Scaling of traces indicated by colorbar. Relative strength of high-frequency noise relative to the low-frequency pulse decays with distance. The low frequency pulse switches polarity along the nerve bundles termination zone. (**C**) shows the fiber density overlayed with the strength of the high-frequency EFP component. (**D**) shows the density of bifurcations and terminations at varying depths.

Axonal projections generate a dipole-like field potential To understand the effect of axon geometry on the EFP, we began by simulating a fiber bundle which runs at constant diameter and without bifurcations, then reaches a bifurcation zone with increasing density, before terminating (Figure 1A). The bundle fibers were stimulated with a background spontaneous rate, upon which a pulse of increased activity was added. The resulting extracellular potential was generated for several locations (Figure 1B). The most salient feature of the response traces is a biphasic deflection evoked by the rate pulse. The deflection is visible at all locations, and its peak-to-peak amplitude is indicated by the color code in figures 1A and 1B.

The low-frequency (eg population rate pulse) parts are governed by the local density of bifurcations and terminations(**Fig 1B**) The high-frequency (eg individual spikes, 'noise', neurophonic) parts are governed by the local fiber density(**Fig 1C**)

- Axonal projections generate a dipole-like field potential (**Fig 1A**)
  - long range
  - low frequency
  - Examples of phenomenology from literature
- General results for axonal projections :
  - The low-frequency (eg population rate pulse) parts are governed by the local density of bifurcations and terminations(**Fig 1B**)
  - The high-frequency (eg individual spikes, 'noise', neurophonic) parts are governed by the local fiber density(**Fig 1C**)
  - The low-frequency component exceeds the high-frequency component in reach (**Fig 2**)
- The barn owl neurophonic as an example that shows these properties(**Fig 3**)
  - The high-frequency component shows a steady increase in latency along the projections' depth, while the low-frequency can have stationary parts caused by sharp increases or decreases of fiber number (bifurcations or terminations).
  - These aspects are reflected in the model
- Ways of understanding the effect
  - Single AP along single axon(**Fig 4**)
  - Analytical model(**Fig 5**)

Discussion

- Relevance of Findings
  - Interpretation of CSD
    * Classical CSD: constant fiber density, variable currents
    * Here: variable fiber density, constant currents
  - Dipole has far field, ABR response?
- Compare to other auditory systems (Chicken NL, MSO)
  - Speculate on functional relevance of polarity shift (a la Rinzel & Goldwyn)
- compare to other fiber bundle systems

Methods

We modeled the axons using NEURON (Hines and Carnevale, 1997; Hines et al., 2009) in a model based on previous work by (**refs**), including the high and low threshold potassium channels used by (**refs**). The axon was modeled as a sequence of active nodes and passive myelinated segments. The parameters for the active and passive segments are described in Table 1. Unlike previous models, we included branching axons in our simulations. These were generated by connecting two passive segments to a node, and continuing the alternation of active and passive segment in each resulting branch.

Action potentials were initiated in the axons by injecting a current pulse into the first node of Ranvier of the axon. The times of the injections were chosen by drawing from an inhomogeneous Poisson distribution based on the firing statistics of NM units in response to a given stimulus.

Axon branching patterns were generated procedurally, **better wording** starting with the root segment, placed at the border of NL. In order to avoid artifacts from the current pulse injection and to simulate the fiber tract leading up to NL, a sequence of 10 active and passive segments without bifurcations was added before the root. To this root, segments were appended iteratively. Before adding a segment, a decision whether to branch or terminate an axon was drawn from a probability distribution dependent on the dorsoventral depth of the end of the previous segment. These probability distributions were modeled as logistic functions with the parameters adjusted to roughly match the numbers of branchings and terminations found in the tracings shown in publications such as Carr and Konishi (1990). This meant that an initial phase of bifurcations was followed by a phase of terminations, with the probability of termination reaching 100% at the end of NL.

The simulations of these axons yielded the membrane currents, from which we calculated the extracellular fields. The procedure for this is described in detail by Gold et al. (2006), among others. Briefly, the extracellular medium is assumed to be a homogeneous volume conductor with conductivity σ_e, and a quasi-static approximation of the electrical field potential ϕ is made. The extracellular potential due to a current distribution $i(\mathbf{r}, t)$ is then governed by the equation $\Delta\phi = \frac{1}{\sigma_e} i(\mathbf{r}, t)$, with Δ denoting the Laplace operator. If the currents i are constrained to a volume V, this equation has the solution:

$$\phi(\mathbf{r}, t) = \frac{1}{4\pi\sigma_e} \int_V \frac{i(\mathbf{r}', t)}{|\mathbf{r} - \mathbf{r}'|} \mathrm{d}\mathbf{r}' \tag{1}$$

Since the currents though the myelinated segments were negligible, and the nodes of Ranvier are small, we used the point source approximation of only the node currents, and did not include the line source approximation used by Holt and Koch (1999).

parameter	value
g_{Na}	0.8 S/cm^2
g_{KLVA}	0.1 S/cm^2
g_{KHVA}	1.5 S/cm^2
C_{mem}	1.0 μF/cm^2

Table 1: Model Parameters **add: leak conductance, myelin parameters, extracellular conductivity sizes**

Simplified axon bundle model

We define the spatial dimension in cylindrical coordinates $\mathbf{r} = (\rho, \varphi, z)$ such that z is the dorsoventral direction, increasing from dorsal to ventral, and $z = 0$ is the dorsal border of NL. We further define $\hat{\mathbf{e}}_z$ as the unit vector in z direction, and $\hat{\mathbf{e}}_\rho$ as an arbitrary unit vector perpendicular to the z direction.

Let us first consider a simple model axon that extends infinitely on both sides and in a straight line from the dorsal direction into NL, and at 0 in the remaining coordinates. Furthermore, we consider

a single action potential propagating along this axon. This axon then has a non-zero current density only at $\rho = 0$, which we denote $i_\infty(z, t)$, meaning that in this case $i(\mathbf{r}, t) = \delta(\rho)i_\infty(z, t)$. Applying this to equation 1, corresponding response $\kappa_\infty(\mathbf{r}, t)$ of an action potential propagating through such a line-axon is then

$$\kappa_\infty(\mathbf{r}, t) = \frac{1}{4\pi\sigma_e} \int_V \frac{\delta(\rho')i_\infty(z', t)}{|\mathbf{r} - \mathbf{r}'|} \mathrm{d}\mathbf{r}' \tag{2}$$

$$= \frac{1}{4\pi\sigma_e} \int_{-\infty}^{\infty} \frac{i_\infty(z', t)}{|\mathbf{r} - z'\hat{\mathbf{e}}_z|} \mathrm{d}z' \tag{3}$$

We will call this response a spike kernel because it will take the role of an integral kernel in the following.

Due to the rotational symmetry, the kernel at a distance ρ from the axon, regardless of φ, can then be described by

$$\kappa_\infty(\mathbf{r}, t) = \frac{1}{4\pi\sigma_e} \int_{-\infty}^{\infty} \frac{i_\infty(z', t)}{|(z - z')\hat{\mathbf{e}}_z + \rho\hat{\mathbf{e}}_\rho|} \mathrm{d}z' \tag{4}$$

$$= \frac{1}{4\pi\sigma_e} \int_{-\infty}^{\infty} \frac{i_\infty(z', t)}{\sqrt{(z - z')^2 + \rho^2}} \mathrm{d}z' \tag{5}$$

Equation 4 has the form of a convolution with a weighting function w:

$$w(\rho, z) = \frac{1}{4\pi\sigma_e} \frac{1}{\sqrt{z^2 + \rho^2}} \tag{6}$$

The convolution can then be written as:

$$\kappa_\infty(\mathbf{r}, t) = [i_\infty(z, t) * w(\rho, z)]_z \tag{7}$$

with the operator $[\cdot * \cdot]_z$ denoting the convolution with respect to the variable z.

The simplest model of a terminating axon will be a semi-infinite axon, where the membrane current flow is simply set to zero beyond the termination point z_{term}. Using the Heaviside step function H we find kernel κ_{term} of a spike in a terminating axon:

$$\kappa_{\mathrm{term}}(\mathbf{r}, t) = [\{H(z_{\mathrm{term}} - z) \cdot i_\infty(z, t)\} * w(\rho, z)]_z \tag{8}$$

Similarly, the model of a bifurcating axon would be one in which the current flow after the bifurcation point z_{bif} is double that of the single infinite fiber.

$$\kappa_{\mathrm{bif}}(\mathbf{r}, t) = [\{(1 + H(z - z_{\mathrm{bif}})) \cdot i_\infty(z, t)\} * w(\rho, z)]_z \tag{9}$$

This places the child branches in superposition at $\rho = 0$, which is a useful approximation for small branching angles.

Approximating terminations and bifurcations in this way disregards the boundary effects that may appear due to the conservation of charge and the inability of charge to flow beyond the termination. However, since the integral over i_∞ is zero for realistic action potentials, the conservation of charge is maintained in the long run.

In more general terms, a coherently stimulated axon bundle with terminations and bifurcations along it's path can be described by the number of individual fibers $n(z)$ at any depth. The extracellular potential κ_b of such a bundle in which the action potential is initiated at the same time and location is then given by

$$\kappa_\mathrm{b}(\mathbf{r}, t) = \left[\{n(z) \cdot i_\infty(z, t)\} * w(\rho, z)\right]_z \tag{10}$$

If we want to calculate the combined field of many axons and action potentials, we can do so by linearly summing the individual axon fields.

If all axons in the bundle are driven with the same the mean firing rate $\lambda(t)$, which might be modulated in time, the field potential $\Phi(\mathbf{r}, t)$ in response to this firing rate will be the (temporal) convolution of the firing rate with the response of the bundle to a coherent spike in all axons:

$$\Phi(\mathbf{r}, t) = \left[\kappa_\mathrm{b}(\mathbf{r}, t) * \lambda(t)\right]_t \tag{11}$$

Substituting equation 10 into equation 11, and taking advantage of the fact that only i_∞ and λ depend on t gives

$$\Phi(\mathbf{r}, t) = \left[\left[\{n(z) \cdot i_\infty(z, t)\} * w(\rho, z)\right]_z * \lambda(t)\right]_t \tag{12}$$

$$= \left[\{n(z) \cdot [i_\infty(z, t) * \lambda(t)]_t\} * w(\rho, z)\right]_z \tag{13}$$

With the average current in a single infinite fiber stimulated with λ, which we will denote it with $i_\lambda(z, t) := [i_\infty(z, t) * \lambda(t)]_t$ this gives us

$$\Phi(\mathbf{r}, t) = \left[\{n(z) \cdot i_\lambda(z, t)\} * w(a, z)\right]_z \tag{14}$$
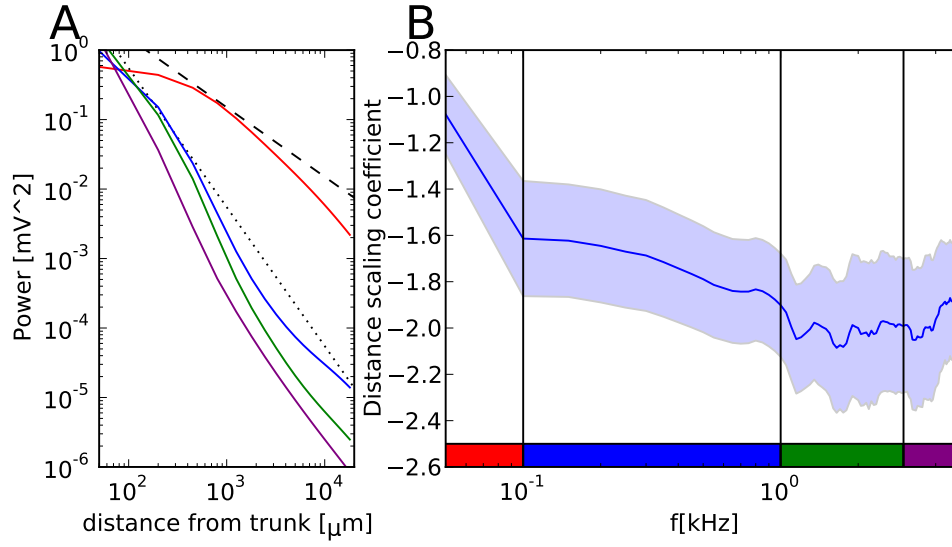
Figure 2: Low-frequency component of the axon bundle EFP exceeds high frequency in reach. (**A**) shows the behaviour of different spectral components (frequency indicated by colorbar) in a double logarithmic plot. The slope indicates the scaling coefficient in this frequency band. (**B**) shows this scaling coefficient for different frequencies. Low frequencies have the least negative coefficient, indicating the furthest reach.
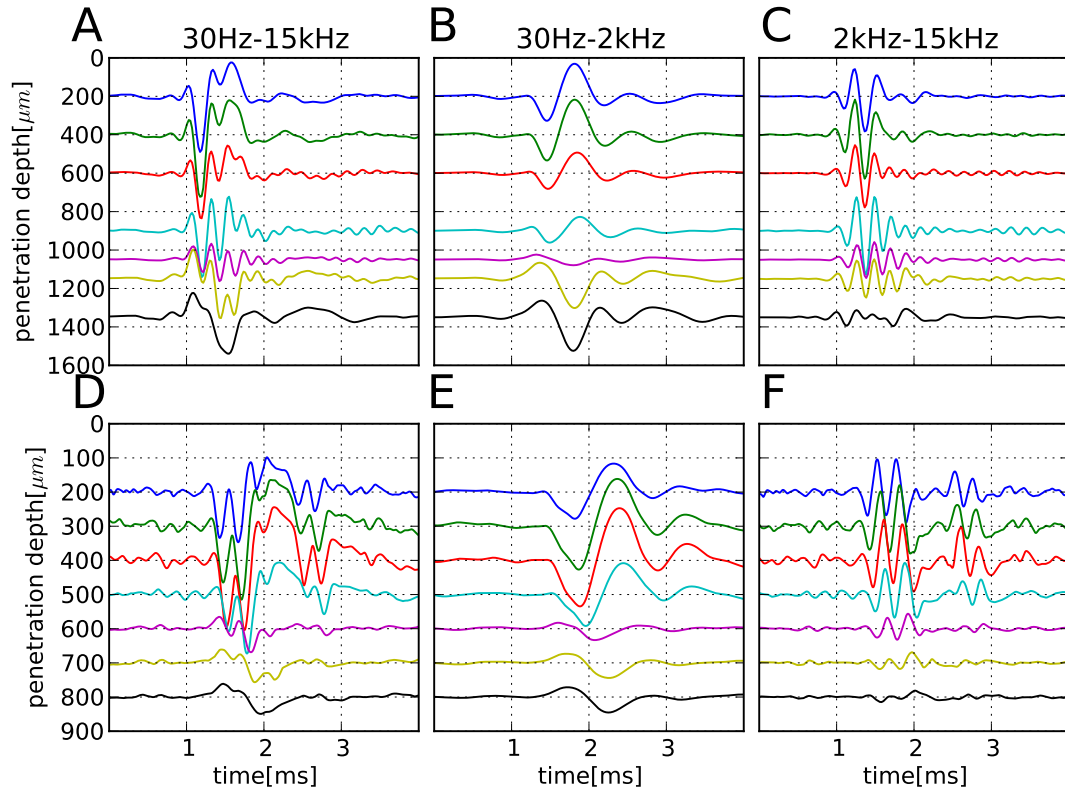
Figure 3: Data from the barn owl shows the expected behaviour predicted by the model. (**A**-**C**) shows data from the barn owls nucleus laminaris in response to an auditory click stimulus, compared to a simulation of the axonal structure and activation in (**D**-**F**). The click stimulus induces a pulse of activity in the afferent axon bundle. The low-frequency components (**B** and **E**) show the polarity reversal. The high frequency component (**C** and **F**), does not show such a reversal, but rather shows a steady increase in phase with depth.
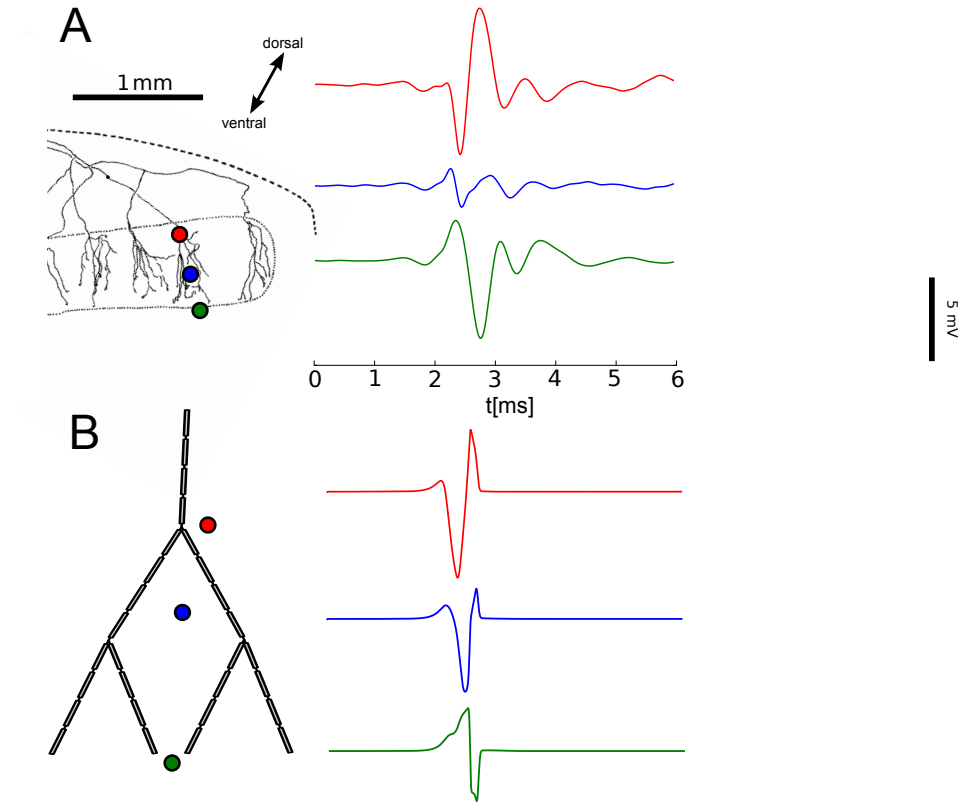
Figure 4: The dipolar behaviour can be understood by examining individual action potentials on a single axon tree. Comparing the low frequency owl data (**A**) to a single axon and action potential in model (**B**) shows a similar behaviour. In particular, the potential at a termination and that at a bifurcation (red and green curves in **B**) are approximately inverted.
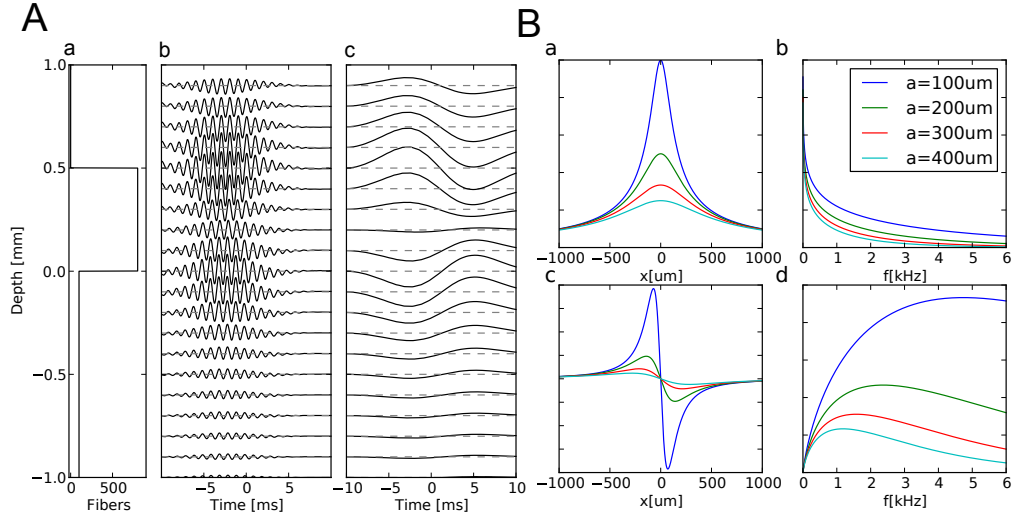
Figure 5: Analytical model of the axon bundle potential explains the effects observed in the numerical model and example data. (**A**) shows the behaviour of a simplified fiber bundle with a piecewise constant fiber density (**Aa**). The high frequency component (**Ab**) shows no polarity reversal, while the high-frequency component (**Ac**) does, as expected from the data and modelling. This can be understood by decomposing the signal into two components. The first component is governed by the bifurcation and termination density, and is filtered by the regular weighting function (**Ba**), which acts as a low-pass filter (**Bb**). The second component is governed by the fiber density, and is filtered by the derivative of the weighting function (**Bc**), which acts as a high- or band-pass filter (**Bd**).

Bibliophraphy

Anastassiou CA, Perin R, Buzsáki G, Markram H, Koch C (2015) Cell type- and activity-dependent extracellular correlates of intracellular spiking. Journal of Neurophysiology 114:608–623 Available at: http://dx.doi.org/10.1152/jn.00628.2014.

Brette R, Destexhe A eds. (2012) Handbook of Neural Activity Measurement. Cambridge: Cambridge University Press. Available at: http://dx.doi.org/10.1017/cbo9780511979958.

Buzsáki G, Anastassiou CA, Koch C (2012) The origin of extracellular fields and currents — EEG, ECoG, LFP and spikes. Nature Reviews Neuroscience 13:407–420 Available at: http://dx.doi.org/10.1038/nrn3241.

Carr CE, Konishi M (1990) A circuit for detection of interaural time differences in the brain stem of the barn owl. The Journal of Neuroscience 10:3227–3246 Available at: http://www.jneurosci.org/content/10/10/3227.abstract.

Denker M, Roux S, Lindén H, Diesmann M, Riehle A, Grün S (2011) The Local Field Potential Reflects Surplus Spike Synchrony. Cerebral Cortex 21:2681–2695 Available at: http://dx.doi.org/10.1093/cercor/bhr040.

Einevoll GT, Kayser C, Logothetis NK, Panzeri S (2013) Modelling and analysis of local field potentials for studying the function of cortical circuits. Nature Reviews Neuroscience 14:770–785 Available at: http://dx.doi.org/10.1038/nrn3599.

Gold C, Henze DA, Koch C, Buzsáki G (2006) On the origin of the extracellular action potential waveform: A modeling study. Journal of neurophysiology 95:3113–3128 Available at: http://dx.doi.org/10.1152/jn.00979.2005.

Goodman CS, Bastiani MJ, Doe CQ, Lac S du, Helfand SL, Kuwada JY, Thomas JB (1984) Cell recognition during neuronal development. Science (New York, NY) 225:1271–1279 Available at: http://view.ncbi.nlm.nih.gov/pubmed/6474176.

Gydikov A, Gerilovsky L, Radicheva N, Trayanova N (1986) Influence of the muscle fibre end geometry on the extracellular potentials. 54:1–8 Available at: http://dx.doi.org/10.1007/bf00337110.

Gydikov AA, Trayanova NA (1986) Extracellular potentials of single active muscle fibres: Effects of finite fibre length. 53:363–372 Available at: http://dx.doi.org/10.1007/bf00318202.

Hentschel HGE, Ooyen A van (1999) Models of axon guidance and bundling during development. Proceedings of the Royal Society of London B: Biological Sciences 266:2231–2238 Available at: http://dx.doi.org/10.1098/rspb.1999.0913.

Hines ML, Carnevale NT (1997) The NEURON Simulation Environment. Neural Computation 9:1179–1209 Available at: http://dx.doi.org/10.1162/neco.1997.9.6.1179.

Hines ML, Davison AP, Muller E (2009) NEURON and Python. Frontiers in neuroinformatics 3 Available at: http://dx.doi.org/10.3389/neuro.11.001.2009.

Holt GR, Koch C (1999) Electrical Interactions via the Extracellular Potential Near Cell Bodies. Journal of Computational Neuroscience 6:169–184 Available at: http://dx.doi.org/10.1023/a:1008832702585.

Kandel ER, Schwartz JH, Jessell TM, Others (2000) Principles of neural science. McGraw-Hill

New York.

Kuokkanen PT, Wagner H, Ashida G, Carr CE, Kempter R (2010) On the origin of the extracellular field potential in the nucleus laminaris of the barn owl (Tyto alba). Journal of neurophysiology 104:2274–2290 Available at: http://dx.doi.org/10.1152/jn.00395.2010.

Lindén H, Pettersen K, Einevoll G (2010) Intrinsic dendritic filtering gives low-pass power spectra of local field potentials. Journal of computational neuroscience 29:423–444 Available at: http://dx.doi.org/10.1007/s10827-010-0245-4.

Lindén H, Tetzlaff T, Potjans TC, Pettersen KH, Grün S, Diesmann M, Einevoll GT (2011) Modeling the Spatial Reach of the LFP. Neuron 72:859–872 Available at: http://dx.doi.org/10.1016/j.neuron.2011.11.006.

Nornes HO, Das GD (1972) Temporal pattern of neurogenesis in spinal cord: cytoarchitecture and directed growth of axons. Proceedings of the National Academy of Sciences of the United States of America 69:1962–1966 Available at: http://view.ncbi.nlm.nih.gov/pubmed/4114859.

Nunez PL, Srinivasan R (2006) Electric Fields of the Brain. Oxford University Press. Available at: http://dx.doi.org/10.1093/acprof:oso/9780195050387.001.0001.

Plonsey R (1977) Action potential sources and their volume conductor fields. Proceedings of the IEEE 65:601–611 Available at: http://dx.doi.org/10.1109/proc.1977.10539.

Rattay F, Danner SM (2014) Peak I of the human auditory brainstem response results from the somatic regions of type I spiral ganglion cells: Evidence from computer modeling. Hearing research 315C:67–79 Available at: http://view.ncbi.nlm.nih.gov/pubmed/25019355.

Reimann MW, Anastassiou CA, Perin R, Hill SL, Markram H, Koch C (2013) A Biophysically Detailed Model of Neocortical Local Field Potentials Predicts the Critical Role of Active Membrane Currents. Neuron 79:375–390 Available at: http://dx.doi.org/10.1016/j.neuron.2013.05.023.

Schomburg EW, Anastassiou CA, Buzsáki G, Koch C (2012) The Spiking Component of Oscillatory Extracellular Potentials in the Rat Hippocampus. The Journal of Neuroscience 32:11798–11811 Available at: http://dx.doi.org/10.1523/jneurosci.0656-12.2012.

Schüz A, Braitenberg V (2002) The Human Cortical White Matter. In: Cortical areas (Schüz A, ed), pp 377–386. Abingdon, UK: Taylor & Francis. Available at: http://dx.doi.org/10.4324/9780203219911/_chapter/_16.